MASS DISTRIBUTION OF WIDE HOT SUBDWARFS

Universität Potsdam

Astronomical Institute of the Czech Academy of Sciences

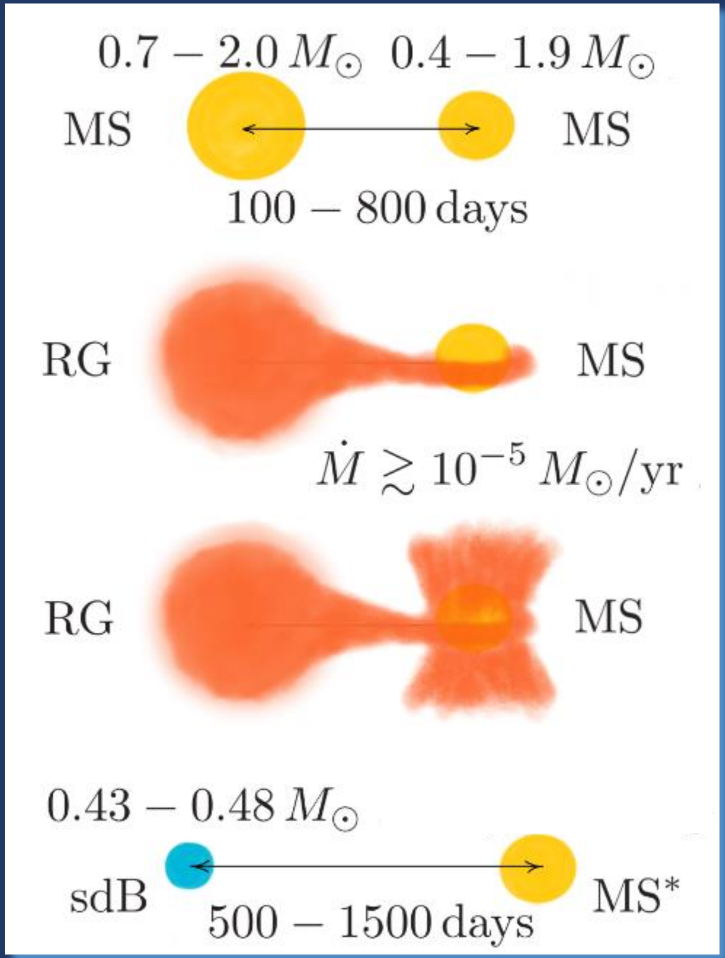

Vos, Bobrick, Vučković; *A&A 641, A163 (2020)*

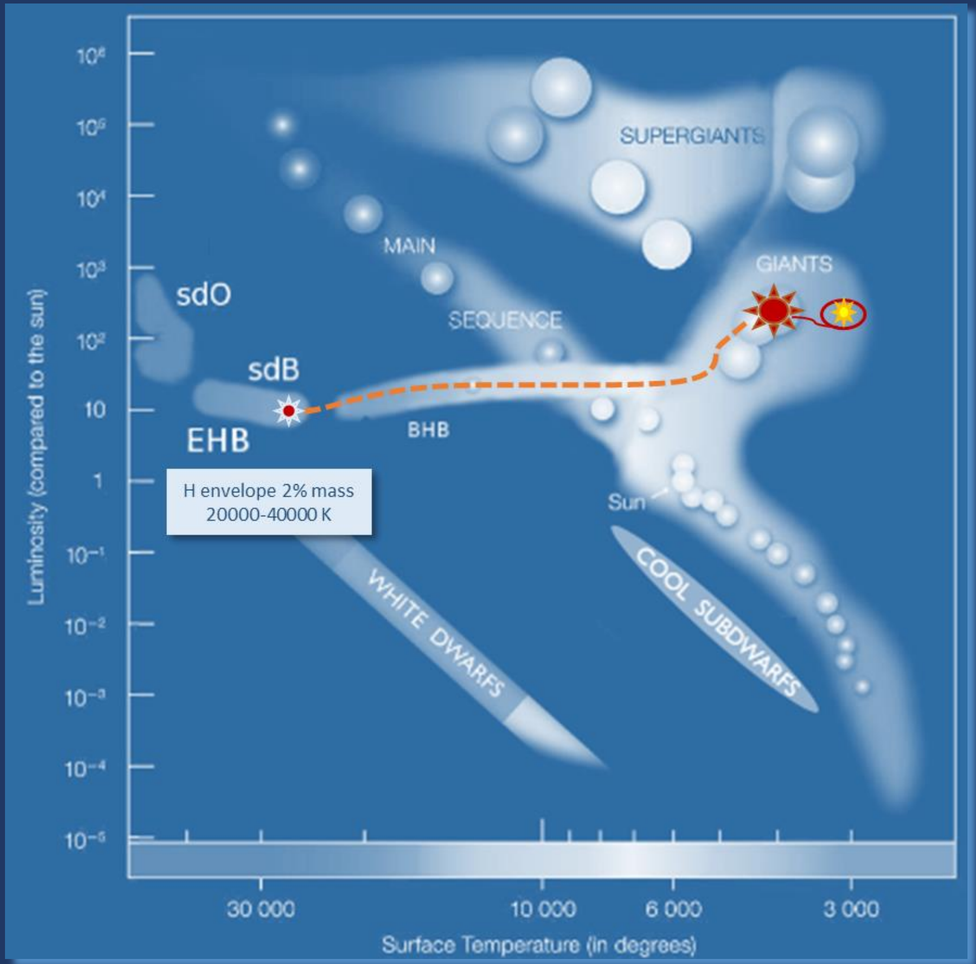

Hot subdwarfs sample Radii & Masses

SPEEDYFIT code

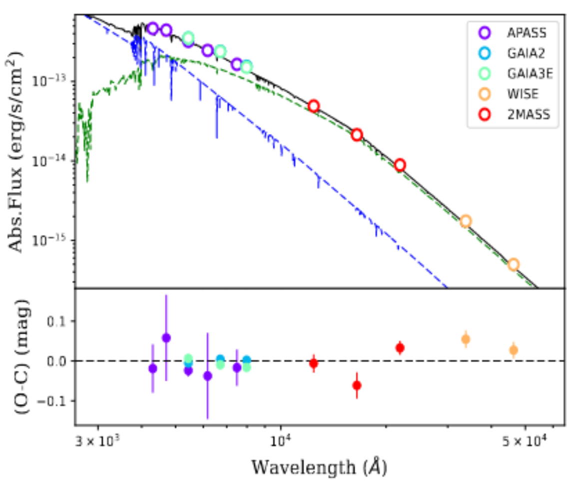

Fig. 2. Photometric SED of the sdB binary system BD+34 1543 obtained from photometry literature by SPEEDYFIT. The solid line in black represents the best-fitting model to the photometry observations. The dashed line in green (MS) and the one in blue (sdB) indicate the best models decomposition for the companion stars of the system. Below is a diagram of residuals (O-C) between photometry and the best composite model.

Molina et al. *in prep. (2024)*

Parallax & q & T_{eff}

Radius
cool star

EMCMASS code

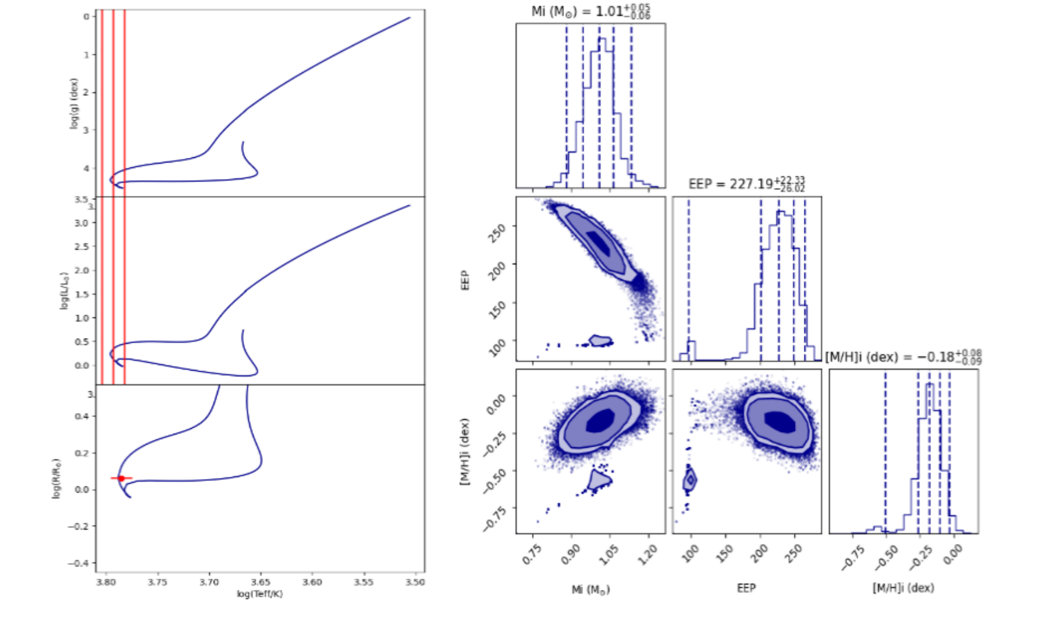

Fig. 3. *Left*: Best fit by EMCMASS of MIST track (in blue line) to the observables of the sdB binary system BD+34 1543 (in red, logT_{eff} and log$R$, including error intervals). *Right*: Parameters estimated by EMCMASS: MS mass, EEP and metallicity.

Molina et al. *in prep. (2024)*

R_{MS} & T_{eff} & [Fe/H]

Mass
cool star

Orbital parameters
(Radial velocity curves)

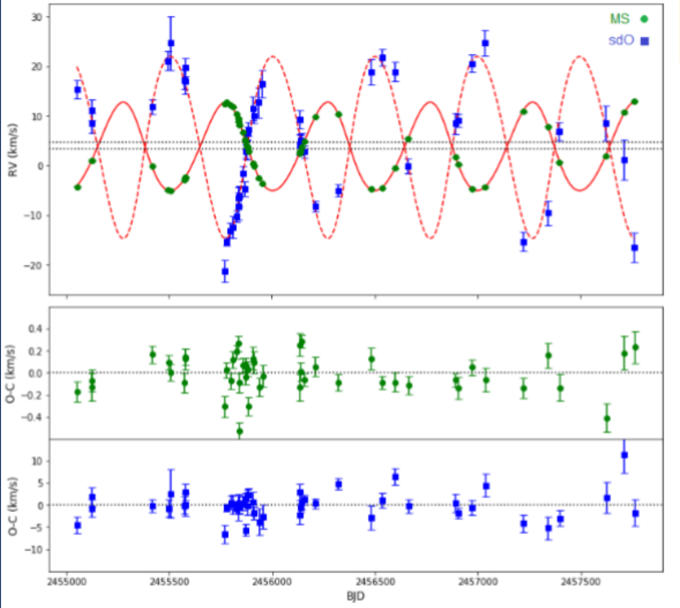

Mass ratio

Parallax

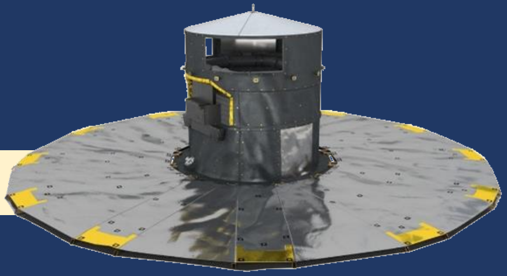

Gaia EDR3

Atmospheric parameters
(GSSP code, LTE models)

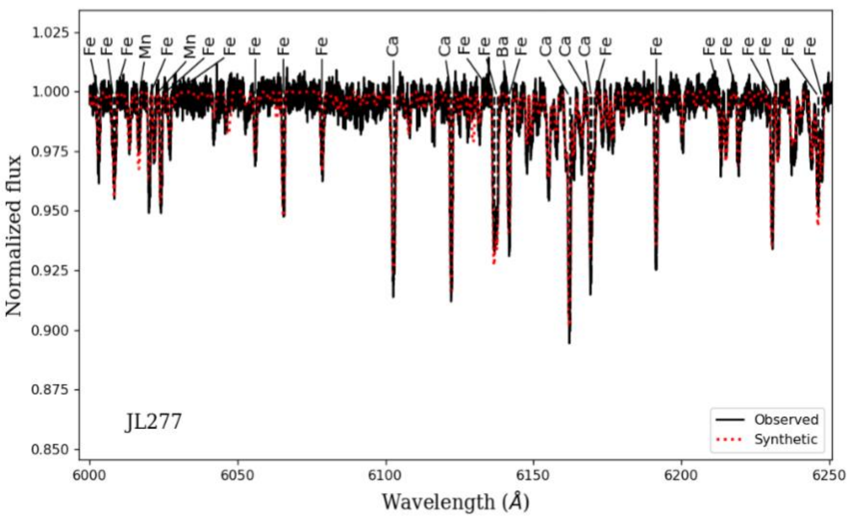

T_{eff} & [Fe/H]

STELLAR ATMOSPHERE MODELS

- Kurucz atmospheric models (LTE) MS
- Tübingen TMAP models (NLTE) sdB

CONSTRAINTS

- Parallax (Gaia EDR3) — Distance, models global scaling to observations
- T_{eff} — Atmospheric parameters (GSSP, Xtgrid)
- Mass ratio (q) — Orbitals parameters

PARAMETERS FITTING (MCMC algorithm)

- $T_{eff\ MS/sdB}$
- Log $g_{\ MS/sdB}$ — Not constrained by SED fit
  Search interval kept fixed or MS range (4.0-5.0 dex)
  Error propagated to SED fit
- E(B-V) — Assumed identical for overall system
  Dust maps not useful for constraining:
  Local not taken into account, RLOF mass loss / CB dust?
- Radius $_{MS}$

Speedyfit Photometry

400 nm 1000 nm 2 µm 3 µm 4 µm 5 µm

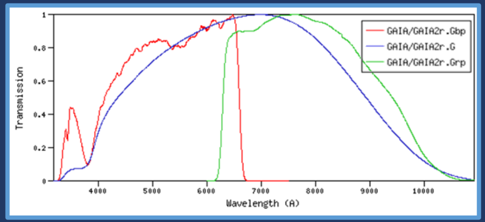

Gaia EDR2
G_{BP} 505 nm
G 625 nm
G_{RP} 774 nm

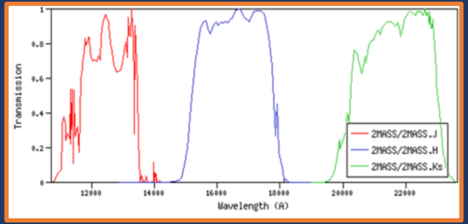

2MASS (NIR)
J 1.23 µm
H 1.66 µm
Ks 2.16 µm

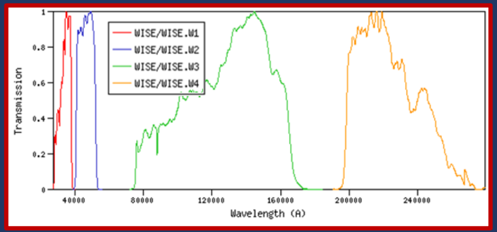

WISE (LWIR-FIR)
W_1 3.35 µm
W_2 4.60 µm
W_3 11.56 µm
W_4 22.09 µm
< DL in sdB

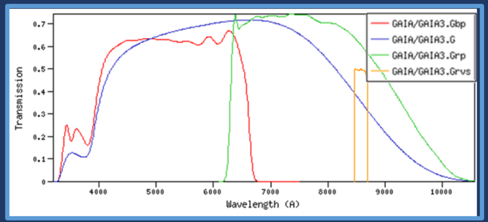

Gaia EDR3
G_{BP} 511 nm
G 622 nm
G_{RP} 777 nm

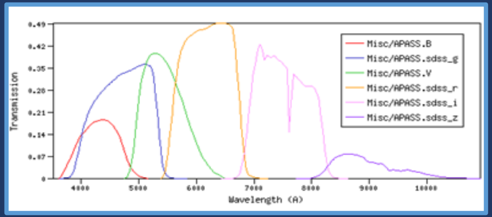

APASS
B 428 nm
V 542 nm
Johnson
g 467 nm
r 616 nm
i 747 nm
SDSS

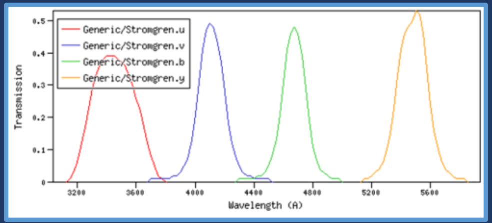

Strömgen
u 344 nm
v 411 nm
b 467 nm
n. a.
y 548 nm
when available

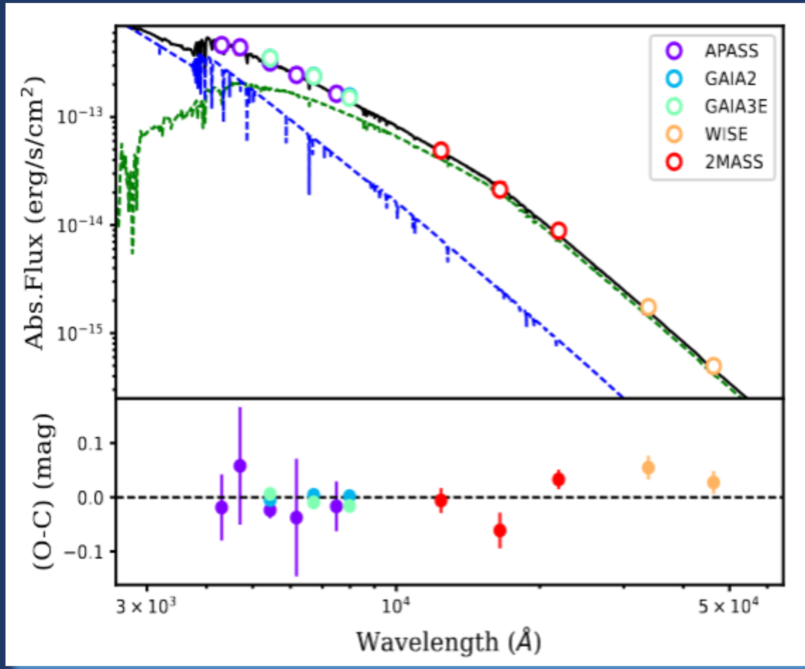

Molina et al. *in prep. (2024)*

Radius
cool star

EMCMASS Models & Parameters

STELLAR EVOLUTION MODELS

- MESA Isochrones & Stellar Tracks (MIST)

OBSERVABLES (MCMC/EMCEE algorithm)

- MS Radius — Speedyfit outcome
- MS T_{eff} — Atmospheric parameters (GSSP, XTgrid)
- MS [Fe/H] — Atmospheric parameters (GSSP, XTgrid)

MS accretion impact during mass exchange?

- 10^{-3} to 10^{-2} $M_{\odot}$ accreted
- Fast homogenization by convective regimen

OUTCOME PARAMETERS

- [Fe/H]
- Equivalent evolutionary phase (EEP)
- MS Mass

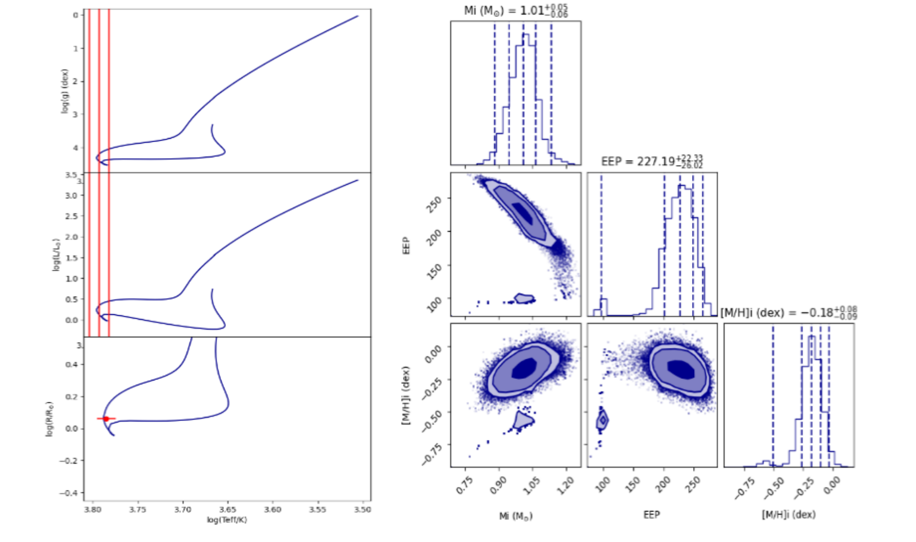

Fig. 3. *Left*: Best fit by EMCMASS of MIST track (in blue line) to the observables of the sdB binary system BD+34 1543 (in red, logT_{eff} and log$R$, including error intervals). *Right*: Parameters estimated by EMCMASS: MS mass, EEP and metallicity.

Molina et al. *in prep. (2024)*

Mass cool star

Verification LEGACY sample

The Astrophysical Journal, 835:172 (31pp), 2017 February 1 doi:10.3847/1538-4357/835/2/172

CrossMark

Standing on the Shoulders of Dwarfs: the *Kepler* Asteroseismic LEGACY Sample. I. Oscillation Mode Parameters

Mikkel N. Lund[1,2], Víctor Silva Aguirre[2], Guy R. Davies[1,2], William J. Chaplin[1,2], Jørgen Christensen-Dalsgaard[2], Günter Houdek[2], Timothy R. White[2], Timothy R. Bedding[2,3], Warrick H. Ball[4,5], Daniel Huber[2,3,6], H. M. Antia[7], Yveline Lebreton[8,9], David W. Latham[10], Rasmus Handberg[2], Kuldeep Verma[2,7], Sarbani Basu[11], Luca Casagrande[12], Anders B. Justesen[2], Hans Kjeldsen[2], and Jakob R. Mosumgaard[2]

The Astrophysical Journal, 835:173 (18pp), 2017 February 1 doi:10.3847/1538-4357/835/2/173

CrossMark

Standing on the Shoulders of Dwarfs: the *Kepler* Asteroseismic LEGACY Sample. II. Radii, Masses, and Ages

Víctor Silva Aguirre[1], Mikkel N. Lund[1,2], H. M. Antia[3], Warrick H. Ball[4,5], Sarbani Basu[6], Jørgen Christensen-Dalsgaard[1], Yveline Lebreton[7,8], Daniel R. Reese[1,2,9], Kuldeep Verma[1,3], Luca Casagrande[10], Anders B. Justesen[1], Jakob R. Mosumgaard[1], William J. Chaplin[1,2], Timothy R. Bedding[1,11], Guy R. Davies[1,2], Rasmus Handberg[1], Günter Houdek[1], Daniel Huber[1,11,12], Hans Kjeldsen[1], David W. Latham[13], Timothy R. White[1], Hugo R. Coelho[2], Andrea Miglio[2], and Ben Rendle[2]

Abstract

We use asteroseismic data from the *Kepler* satellite to determine fundamental stellar properties of the 66 main-sequence targets observed for at least one full year by the mission. We distributed tens of individual oscillation frequencies extracted from the time series of each star among seven modeling teams who applied different methods to determine radii, masses, and ages for all stars in the sample. Comparisons among the different results reveal a good level of agreement in all stellar properties, which is remarkable considering the variety of codes, input physics, and analysis methods employed by the different teams. Average uncertainties are of the order of ~2% in radius, ~4% in mass, and ~10% in age, making this the best-characterized sample of main-sequence stars available to date. Our predicted initial abundances and mixing-length parameters are checked against inferences from chemical enrichment laws $\Delta Y/\Delta Z$ and predictions from 3D atmospheric simulations. We test the accuracy of the determined stellar properties by comparing them to the Sun, angular diameter measurements, *Gaia* parallaxes, and binary evolution, finding excellent agreement in all cases and further confirming the robustness of asteroseismically determined physical parameters of stars when individual frequencies of oscillation are available. Baptised as the *Kepler* dwarfs LEGACY sample, these stars are the solar-like oscillators with the best asteroseismic properties available for at least another decade. All data used in this analysis and the resulting stellar parameters are made publicly available for the community.

Seven pipelines/methods for obtaining stellar radius/mass/age

Table 1
Summary of Codes, Input Physics, and Optimization Methods Applied by Each Pipeline

	AIMS	ASTFIT	BASTA	C2kSMO	GOE	V&A	YMCM
Models	MESA	ASTEC	GARSTEC	Cesam2k	MESA	MESA	YREC
Frequencies	InversionKit	ADIPLS	ADIPLS	LOSC	ADIPLS	ADIPLS	AB94
Solar mixture	GN93	GN93	GS98	GN93	GS98	GS98	GS98
Opacities	OPAL96+JF05	OPAL96+JF05	OPAL96+JF05	OPAL96+JF05	OPAL96 +JF05	OP05+JF05	OPAL96 +JF05
EOS	OPAL05	OPAL05	OPAL05	OPAL05	OPAL05	OPAL05	OPAL05
Nuclear reactions	NACRE	NACRE	NACRE	NACRE	NACRE	NACRE	Solar fusion
Atmosphere	Eddington gray	Eddington gray	Eddington gray	Eddington gray	Eddington gray	Eddington gray	Eddington gray
Diffusion	No	MP93, $\leqslant 1.1\ M_\odot$	T94, $\leqslant 1.2\ M_\odot$	MP93	T94	T94, $\leqslant 1.35\ M_\odot$	No
Overshoot	Yes	No	Yes	Yes	Yes	Yes	Yes
Convection	CG68	MTL58	MLT12	CGM96	CG68	MLT58	MTL58
$\alpha_{\rm conv}$	1.8	1.5, 1.8, 2.1	1.791	Variable	Variable	Variable	Variable
$\Delta Y/\Delta Z$	2.0	1.0–2.0	1.4	Variable	Variable	Variable	Variable
Fitted data	$\nu_i(n)$	$\nu_i(n)$	r_{010}, $r_{02}(n)$	r_{010}, $r_{02}(n)$, $\nu_0(n_{\rm min})$	$\nu_i(n)$	$\langle\Delta\nu\rangle$, $\langle r_{02}\rangle$, $r_{01}(n)$, $r_{10}(n+3)$	$\nu_i(n)$, r_{010}, $r_{02}(n)$
Surface correction	BG14	SC	None	TS15	BG14	HK08	BG14
Optimization	MCMC	χ^2 minimization	Bayesian	Levenberg–Marquardt	Downhill simplex	χ^2 minimization	Monte Carlo
Reference	Appendix A	VSA15	VSA15	LG14	TA15	TA15	VSA15

66 MS known radii and masses from asteroseismic data

Uncertainties:

- Radii: up to 2%
- Masses: up to 4%

SPECTROSCOPIC (LEGACY)

2.2. Atmospheric and Stellar Parameters

We have obtained atmospheric parameters from the Stellar Parameters Classification tool (SPC; see Buchhave et al. 2012), with data from the Tillinghast Reflector Echelle Spectrograph (TRES; Szentgyorgyi & Furész 2007; Fürész 2008) on the 1.5-m Tillinghast telescope at the F. L. Whipple

Buchhave, L. A. & Latham, D. W. *ApJ, 808, 187 (2015)*

54 systems, spectroscopic TRES

KIC	Popular Name	Kp (mag)	ν_{max} (μHz)	$\Delta\nu$ (μHz)	Number of Modes	Category	Braketing Quarters	Missing Quarters	T_{eff} (K)	[Fe/H] (dex)
6603624	Saxo	9.09	2384	110.1	44	Simple	5.1–17.2	...	5674 ± 77	0.28 ± 0.10
6679371	...	8.73	942	50.6	55	F-like	5.1–17.2	...	6479 ± 77	0.01 ± 0.10
6933899	Fred	9.62	1390	72.1	39	Simple	5.1–17.2	...	5832 ± 77	−0.01 ± 0.10
7103006	...	8.86	1168	59.7	54	F-like	5.1–17.2	...	6344 ± 77	0.02 ± 0.10
7106245	...	10.79	2398	111.4	24	Simple	5.1–15.3	...	6068 ± 102(3)	−0.99 ± 0.19(3)

PHOTOMETRIC (SAGA Proj.)

mark for Galactic studies. Similar to our latest revision of the GCS (Casagrande et al. 2011), we combine Strömgren metallicities with broadband photometry to obtain effective temperatures (T_{eff}) and metallicities ([Fe/H]) for all our targets via the infrared flux method (IRFM). This facilitates the task of placing SAGA

Casagrande L., Silva Aguirre V., Stello D., et al. *ApJ, 787, 110 (2014)*

12 systems, contraints from several bibliographic sources (spec/photo)

Verification Radii

Molina et al. *in prep. (2024)*

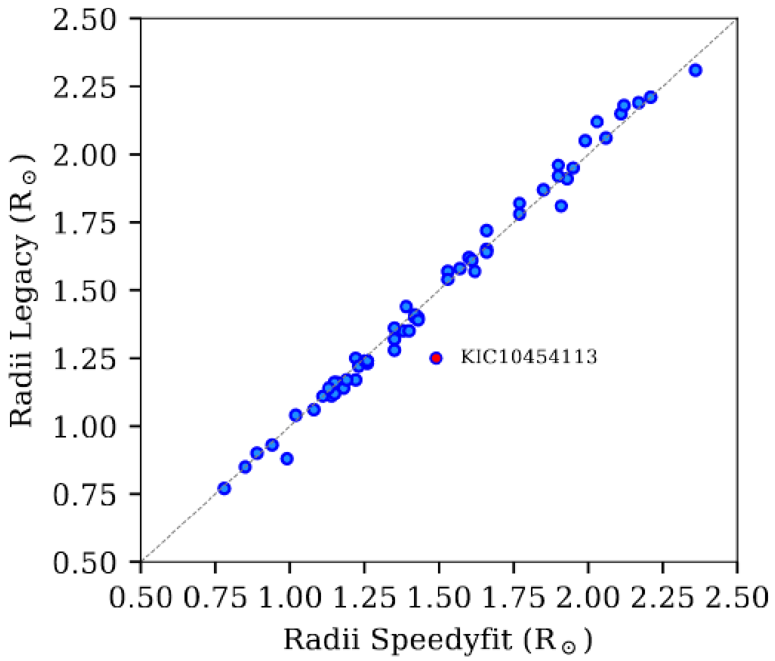

Fig. 4. The estimated radii using the methods based on asteroseismology or photometry data (SPEEDYFIT). The most discrepant result exhibiting a difference greater than 0.2 $R_\odot$ is denoted in red. Error intervals are not significant and not included.

All	$0.01 \pm 0.05\ R_\odot$
KIC10454113 excl.	$0.00 \pm 0.04\ R_\odot$

Verification Radii

Molina et al. *in prep. (2024)*

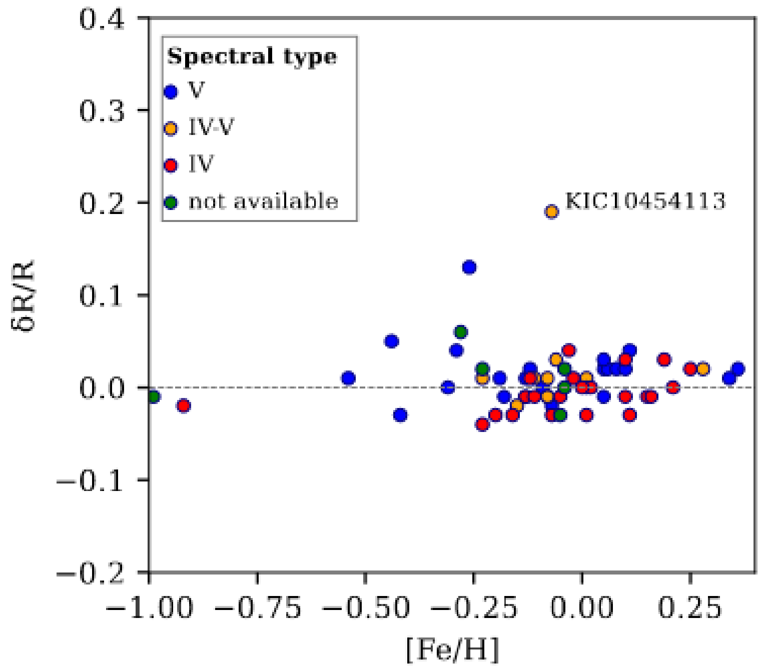

Fig. 5. The fractional differences of derived radii versus metallicity, using methods based on asteroseismology or photometry data (SPEEDYFIT), the first as a reference. Spectral types of information by *SIMBAD*, in colors, are declared in the legend. For clarity, error bars are not included.

All	$0.01 \pm 0.05\ R_\odot$
KIC10454113 excl.	$0.00 \pm 0.04\ R_\odot$

No trend with respect to [Fe/H]

Verification Masses

Molina et al. *in prep. (2024)*

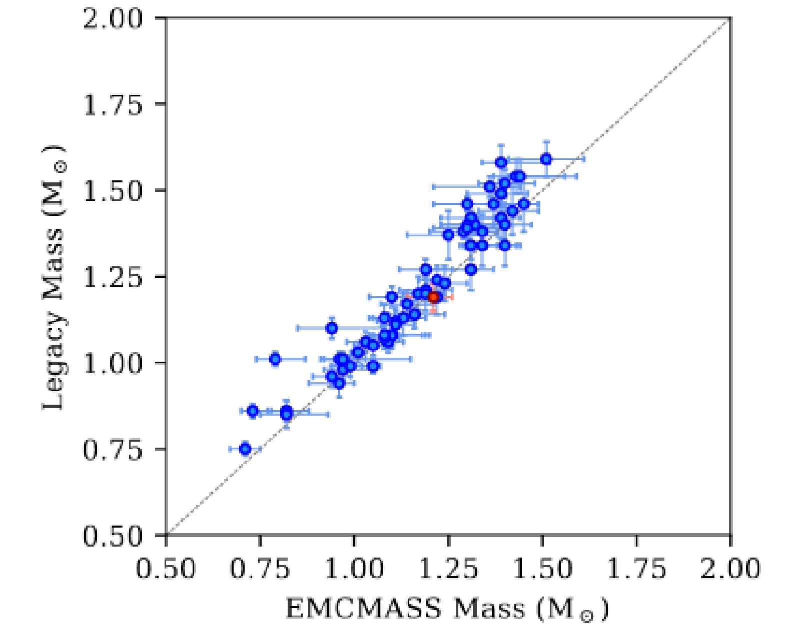

Fig. 6. The estimated masses using the methods based on asteroseismology or photometry data (EMCMASS). In red, the mass of the system KIC10454113 with the most discrepant radius in the previous step.

LEGACY sample differences $-0.04 \pm 0.06\ M_\odot$

Molina et al. *in prep. (2024)*
Bellinger et al. *A&A 622, A130 (2019)*

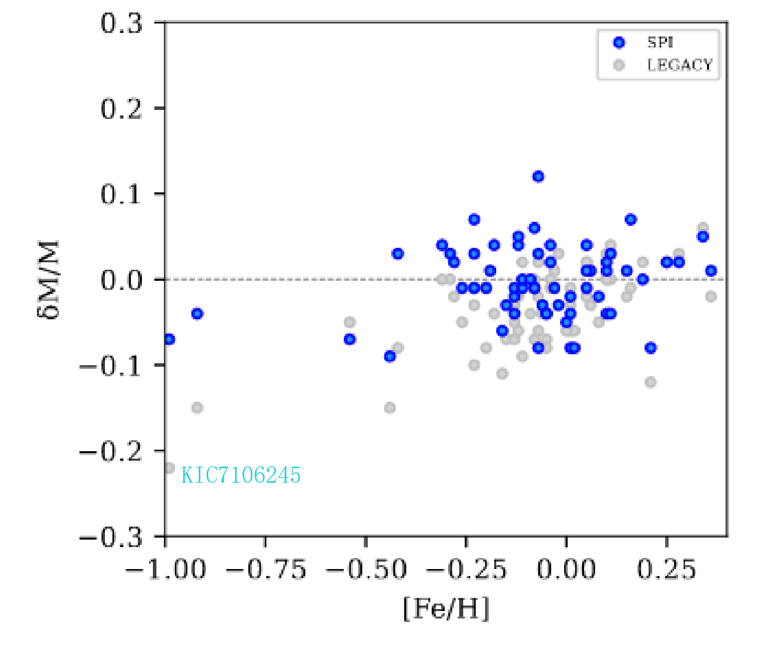

Fig. 11. The fractional differences of derived masses by the method (EMCMASS), taking as main reference the results from the *LEGACY* paper or the derived using an asteroseismic modelling method by Bellinger et al. (SPI, 2019) upon the *LEGACY* sample. For clarity, error bars are not included.

SPI differences $0.00 \pm 0.04\ \delta M/M$

Verification Masses

Molina et al. *in prep. (2024)*
Serenelli et al. *ApJS 223, 23 (2017)*

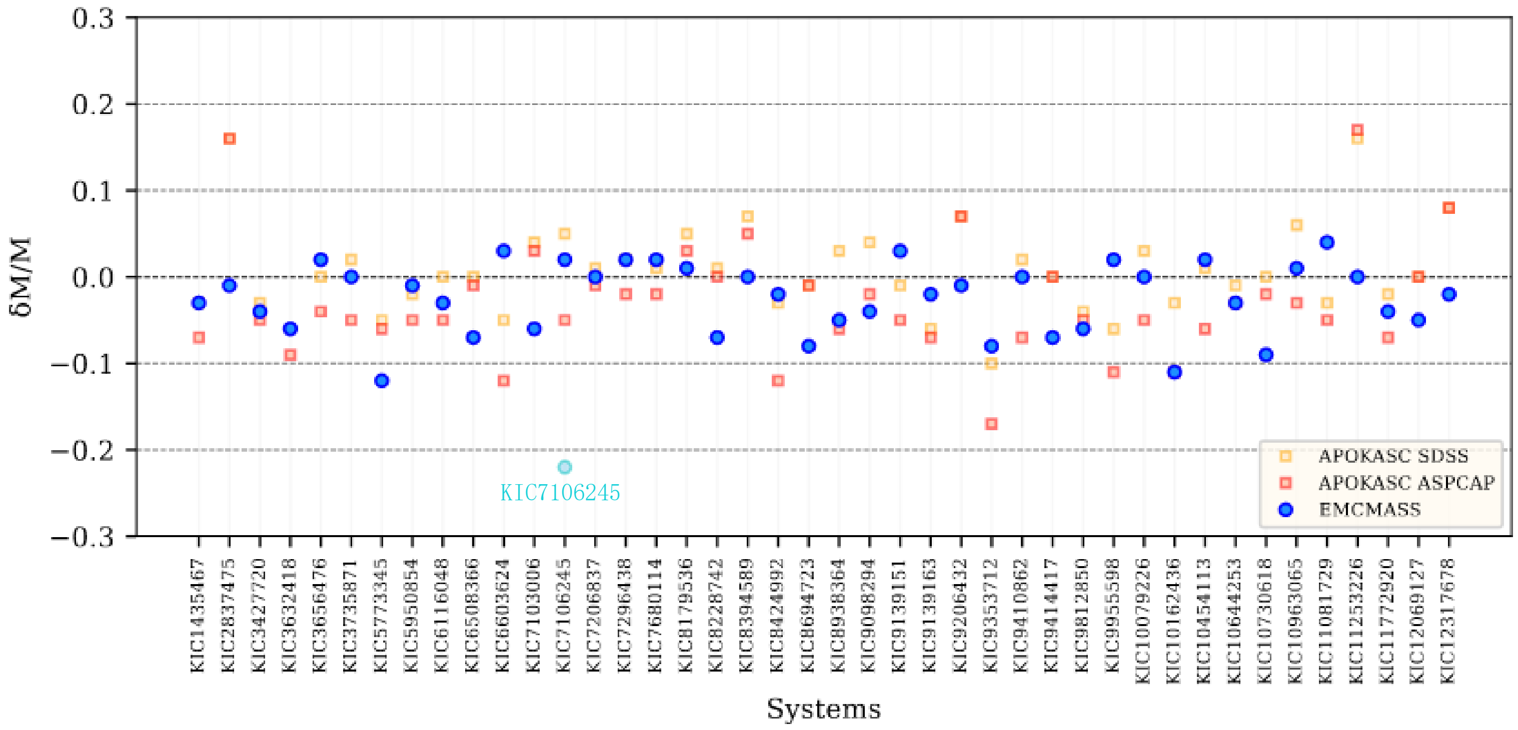

Fig. 10. The mass fractional differences of this study and the ones attained by Serenelli et al. (2017) in their APOKASC catalog with respect to the common KEPLER systems of the LEGACY sample. Two scales were used for the T_{eff} inputs by the authors, based on photometry (*griz* SDSS filters) or spectroscopic data (APOGEE-ASPCAP). Regarding the two values provided by EMCMASS (in blue and skyblue) concerning the metallicity issue of KIC7106245, see text (Sect. 3.3). For clarity, error bars are not included.

KIC7106245

Teff	log.g	Fe_H	c	CompStar	CatNo	Reference
6014	4.29					2020A&A...636A..85S
6020	4.33	-0.19		SUN		2017ApJ...838...25G
5779	4.318					2017ApJS..233...23S
6074	4.333					2017ApJS..233...23S
6078	4.327					2017A&A...601A..67C
5951	4.31	-0.12		SUN		2016ApJS..225...32B

LEGACY 1.01 $M_\odot$
[Fe/H] −0.99 Photom. study 0.79 $M_\odot$
[Fe/H] −0.19 1.03 $M_\odot$

Molina et al. *in prep. (2024)*
Fernandes et al. *A&A 647, A90 (2021)*

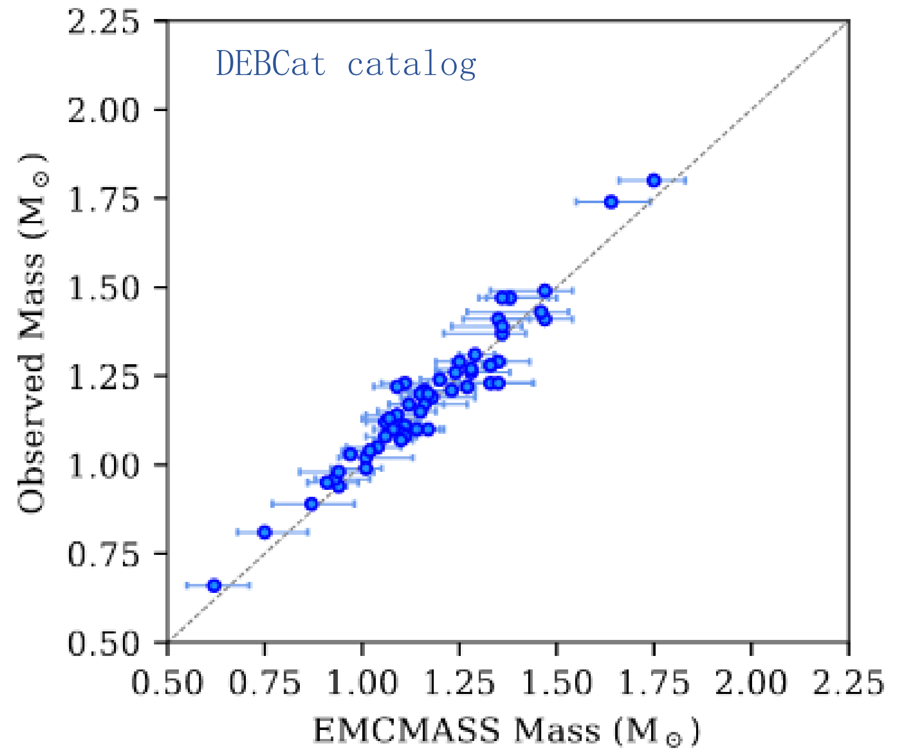

Fig. 12. Observed versus estimated stellar masses by EMCMASS of the selected eclipsing MS binary stars (Fernandes et al. 2021). Included error bars.

Eclipsing binaries sample differences $-0.02 \pm 0.05\ M_\odot$

Wide hot sdB sample

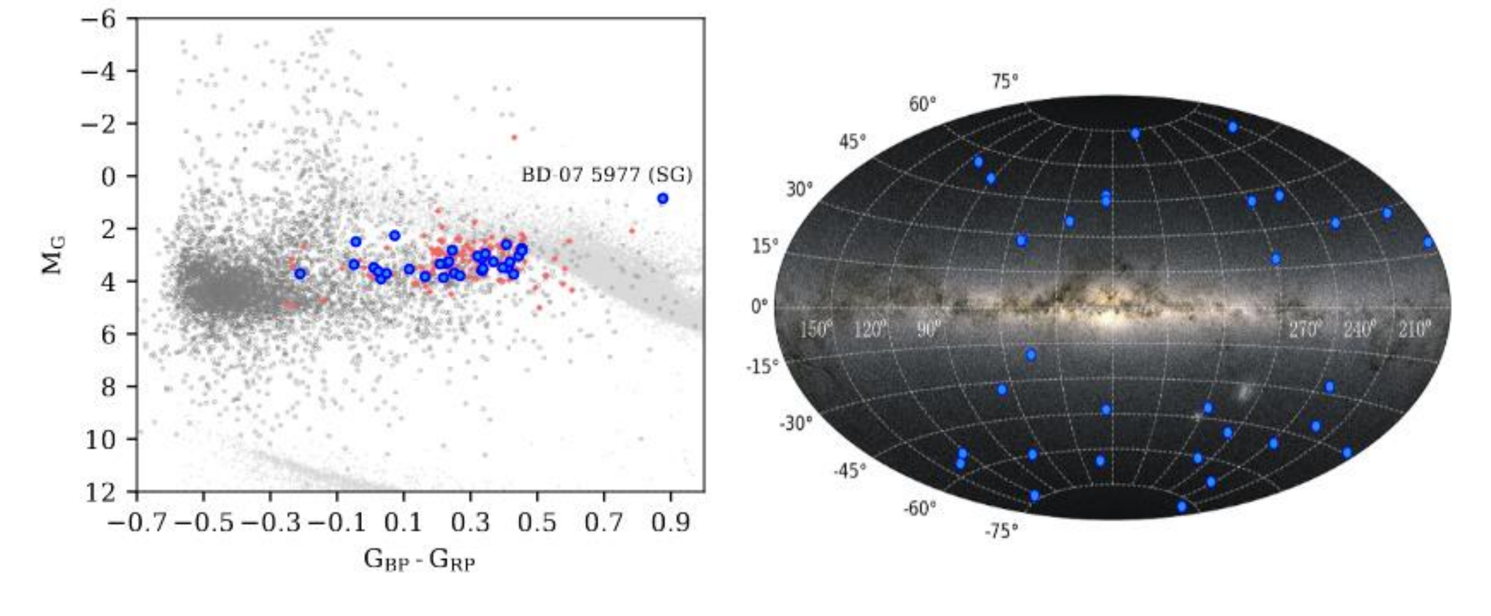

Fig. 13. *Left*: The color-magnitude diagram presented by Pelisoli et al. (2020) regarding their composite hot subdwarfs sample, as dimmed red diamonds, whose light-curves and rotation periods were studied by the authors. We have included the wide hot sdB binary sample with orbital parameter fully solved as blue-filled circles. Stars cataloged by Geier (2020) as hot subdwarfs are represented as dark gray open circles. Main sequence and other evolutionary stage stars within the region from Lindegren et al. (sample C, 2018), are depicted as pale gray dots.
Right: An Aitoff projection displaying the Galactic coordinates of the wide hot sdB sample. The Galactic longitude increases from the center towards the left, incremented by 30° per tick.

Molina et al. *in prep. (2024)*

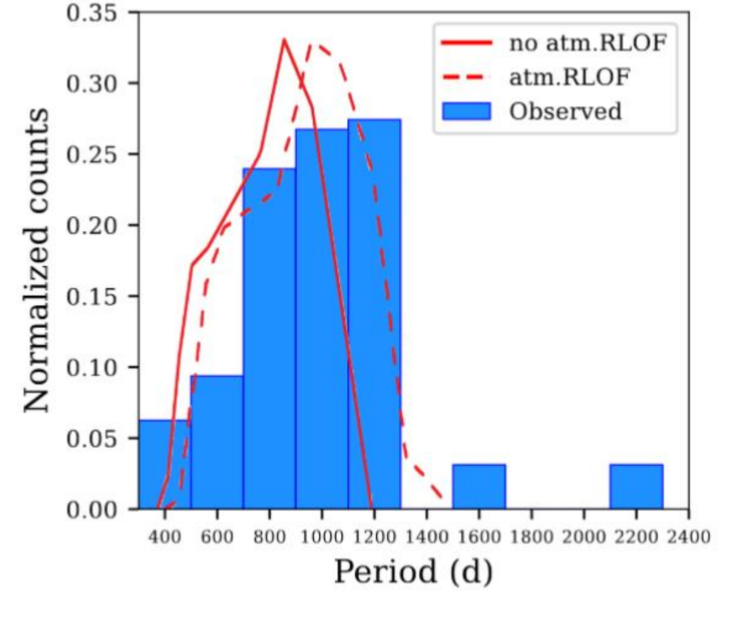

Fig. 14. The distribution-histogram of orbital periods of the wide hot sdB sample. The figure is adapted from Vos et al. (2019) and has been updated with the new solved systems since then. The same method has been employed as outlined in their paper. The predicted period distributions of the BPS studies of Chen et al. (2013), with and without atmospheric RLOF effect, are included.

Molina et al. *in prep. (2024)*

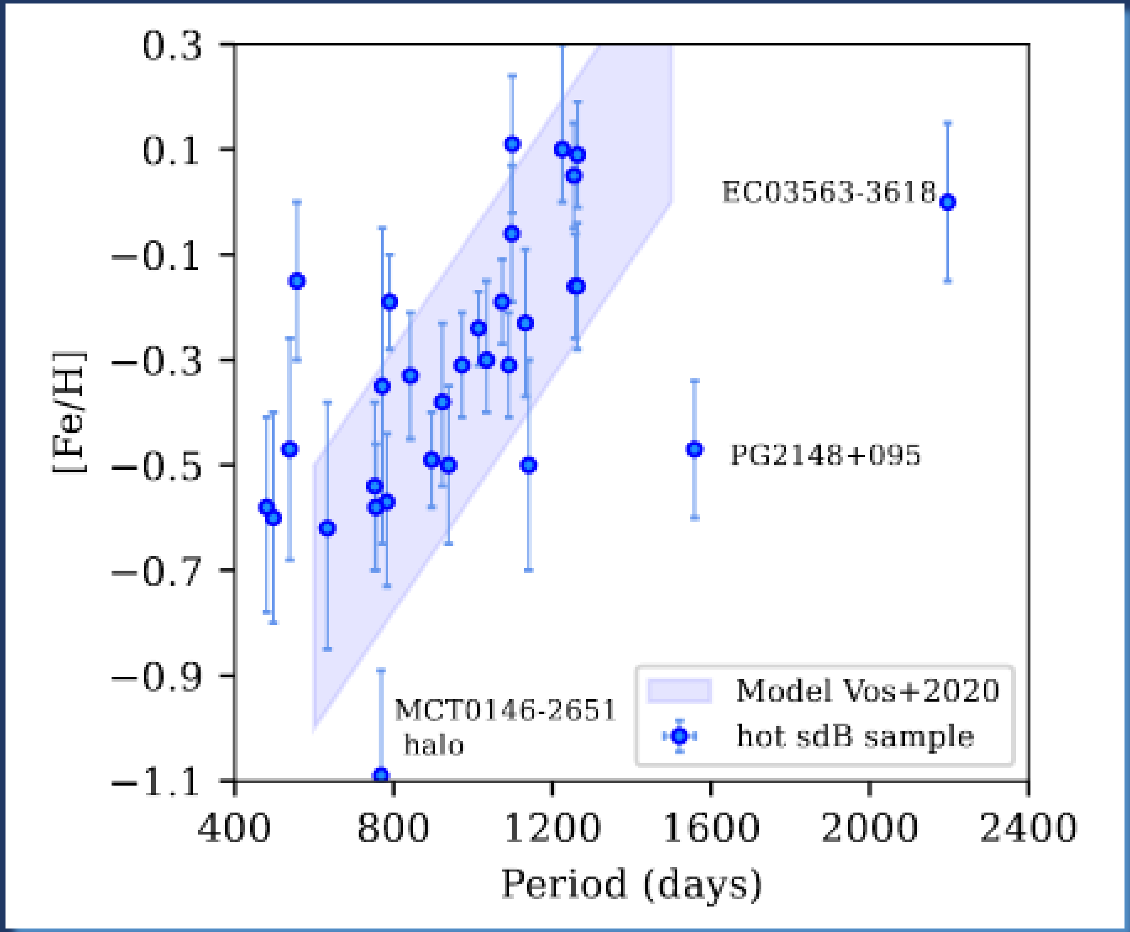

Molina et al. *in prep. (2024)*
Vos, Bobrick, Vučković; *A&A 641, A163 (2020)*

Universität Potsdam
Astronomical Institute of the Czech Academy of Sciences

Our constraints

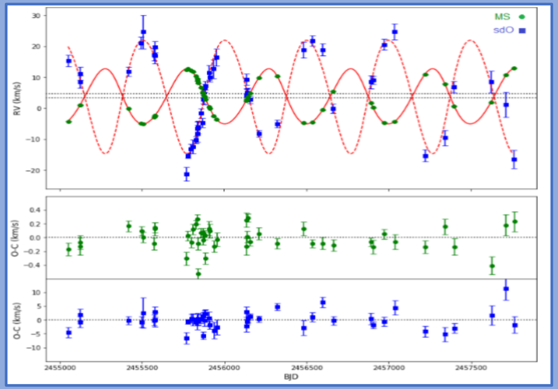

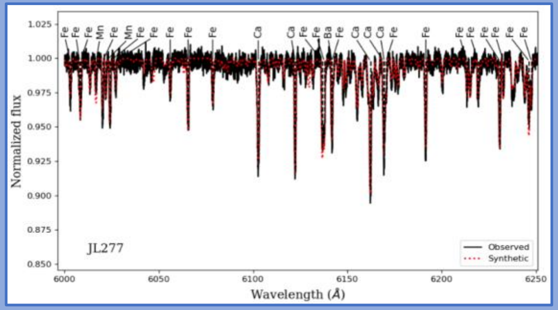

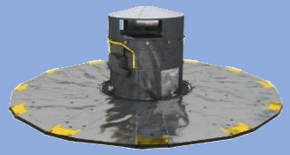

SPEEDYFIT code

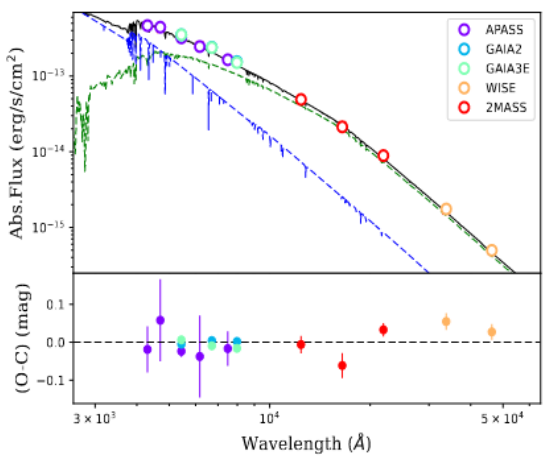

Fig. 2. Photometric SED of the sdB binary system BD+34 1543 obtained from photometry literature by SPEEDYFIT. The solid line in black represents the best-fitting model to the photometry observations. The dashed line in green (MS) and the one in blue (sdB) indicate the best models decomposition for the companion stars of the system. Below is a diagram of residuals (O-C) between photometry and the best composite model.

Parallax & q & T_{eff}

Radius
cool star

EMCMASS code

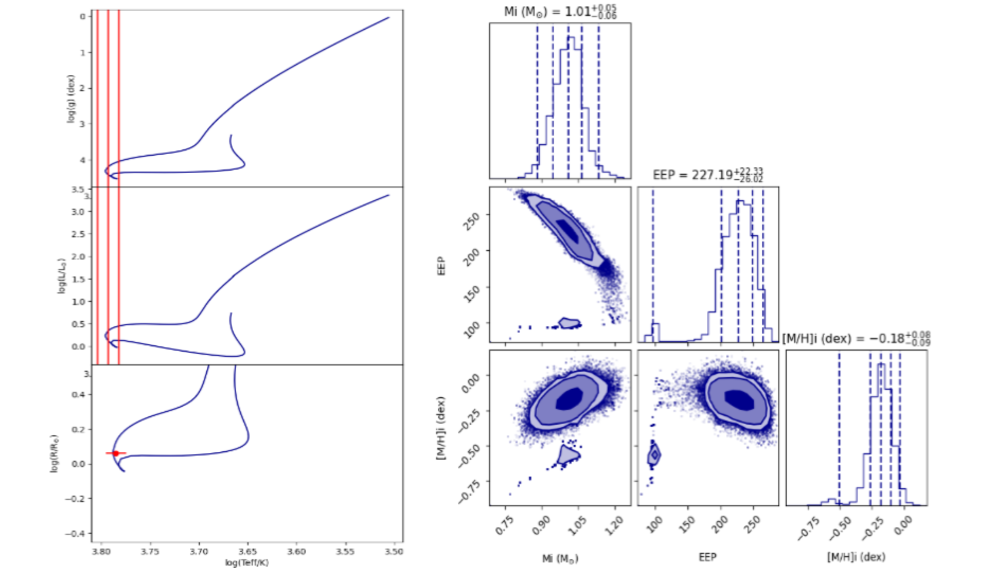

Fig. 3. *Left*: Best fit by EMCMASS of MIST track (in blue line) to the observables of the sdB binary system BD+34 1543 (in red, $\log T_{eff}$ and $\log R$, including error intervals). *Right*: Parameters estimated by EMCMASS: MS mass, EEP and metallicity.

R_{MS} & T_{eff} & [Fe/H]

Mass
cool star

Hot subdwarfs Radii & Masses

Astronomical Institute of the Czech Academy of Sciences

Table 4. MS radii and masses, mass ratios and estimated subdwarf masses obtained for the sample of wide hot subdwarf binary systems. The system BPS CS 22937-0067, given the poor constraint of the mass ratio parameter, does not provide a reliable subdwarf mass. Error intervals included.

Systems	Radius ($R_\odot$)	Mass ($M_\odot$)	Mass ratio (q)	sd Mass ($M_\odot$)
PG 0048+091	0.98 ±0.04	1.03 $^{+0.05}_{-0.11}$	0.539 ±0.093	0.56 $^{+0.10}_{-0.11}$
BD-11 162	1.00 $^{+0.05}_{-0.04}$	0.79 $^{+0.10}_{-0.09}$	0.484 ±0.015	0.38 ±0.05
PB 6355	1.06 ±0.04	1.14 ±0.03	0.360 ±0.017	0.41 ±0.02
SB 744	0.84 ±0.03	0.74 $^{+0.11}_{-0.10}$	0.646 ±0.028	0.48 ±0.07
Faust 321	1.44 $^{+0.03}_{-0.04}$	1.31 ±0.04	0.446 ±0.015	0.58 ±0.03
JL 277	1.18 ±0.04	1.20 $^{+0.04}_{-0.07}$	0.411 ±0.010	0.49 $^{+0.02}_{-0.03}$
GALEX J022836.7-362543	1.17 ±0.03	0.84 $^{+0.10}_{-0.06}$	0.529 ±0.033	0.44 $^{+0.06}_{-0.04}$
EC 03143-5945	1.12 ±0.04	1.01 $^{+0.09}_{-0.08}$	0.428 ±0.009	0.43 ±0.04
GALEX J033216.7-023302	1.70 $^{+0.05}_{-0.10}$	1.51 $^{+0.08}_{-0.07}$	0.347 ±0.009	0.52 ±0.03
EC 03563-3618	1.91 $^{+0.08}_{-0.07}$	1.32 $^{+0.09}_{-0.08}$	0.324 ±0.006	0.43 $^{+0.03}_{-0.03}$
HE 0430-2457	1.89 ±0.22	0.82 $^{+0.10}_{-0.05}$	0.296 ±0.019	0.24 $^{+0.03}_{-0.02}$
GALEX J053939.1-283329	1.06 $^{+0.05}_{-0.04}$	0.83 $^{+0.08}_{-0.07}$	0.686 ±0.053	0.57 ±0.07
BD+34 1543	1.15 $^{+0.02}_{-0.03}$	1.01 $^{+0.05}_{-0.06}$	0.546 ±0.011	0.55 ±0.03
GALEX J081110.8+273420	1.13 ±0.03	1.13 $^{+0.07}_{-0.06}$	0.564 ±0.108	0.64 ±0.13
SDSS J090001.54+012850.5	1.40 $^{+0.04}_{-0.04}$	1.29 $^{+0.09}_{-0.13}$	0.422 ±0.038	0.54 $^{+0.06}_{-0.07}$
GALEX J101703.6-335502	1.21 $^{+0.03}_{-0.04}$	1.12 $^{+0.07}_{-0.05}$	0.370 ±0.023	0.41 $^{+0.04}_{-0.03}$
PG 1018-047	0.96 $^{+0.11}_{-0.08}$	0.56 $^{+0.05}_{-0.04}$	0.664 ±0.039	0.37 $^{+0.04}_{-0.03}$
EC 11031-1348	1.49 $^{+0.02}_{-0.03}$	1.36 $^{+0.12}_{-0.13}$	0.358 ±0.017	0.49 ±0.05
PG 1104+243	0.89 ±0.02	0.83 $^{+0.08}_{-0.06}$	0.697 ±0.023	0.58 $^{+0.06}_{-0.05}$
Feige 80	1.19 $^{+0.06}_{-0.05}$	1.02 ±0.12	0.413 ±0.023	0.42 ±0.05
Feige 87	0.94 $^{+0.05}_{-0.04}$	0.77 $^{+0.09}_{-0.08}$	0.573 ±0.011	0.44 ±0.05
Balloon 82800003	1.26 $^{+0.09}_{-0.11}$	1.22 ±0.08	0.545 ±0.027	0.66 ±0.05
EGGR 440	1.05 ±0.04	0.82 $^{+0.11}_{-0.09}$	0.574 ±0.020	0.47 $^{+0.07}_{-0.05}$
BPS BS 16559-0077	0.85 ±0.03	0.95 $^{+0.04}_{-0.06}$	0.744 ±0.061	0.71 ±0.07
GALEX J162842.0+111838	1.26 ±0.03	1.19 $^{+0.05}_{-0.06}$	0.595 ±0.141	0.71 ±0.17
GALEX J173651.2+280635	1.17 $^{+0.04}_{-0.06}$	1.16 $^{+0.07}_{-0.10}$	0.514 ±0.015	0.60 $^{+0.04}_{-0.05}$
BD+29 3070	1.45 $^{+0.02}_{-0.03}$	1.23 $^{+0.08}_{-0.09}$	0.393 ±0.023	0.48 $^{+0.04}_{-0.05}$
GALEX J202216.8+015225	1.03 ±0.02	1.09 $^{+0.03}_{-0.11}$	0.544 ±0.040	0.59 $^{+0.05}_{-0.07}$
BPS CS 22937-0067	1.42 $^{+0.08}_{-0.05}$	1.23 $^{+0.06}_{-0.07}$	***	***
PG 2148+095	1.61 $^{+0.08}_{-0.07}$	1.21 $^{+0.10}_{-0.08}$	0.474 ±0.046	0.57 ±0.07
EC 22540-3324	2.23 ±0.06	0.99 $^{+0.29}_{-0.14}$	0.639 ±0.030	0.63 $^{+0.19}_{-0.09}$
BD-07 5977	7.84 $^{+0.18}_{-0.16}$	1.48 $^{+0.47}_{-0.32}$	0.423 ±0.068	0.63 $^{+0.22}_{-0.17}$

Molina et al. *in prep. (2024)*

Molina et al. *in prep. (2024)*

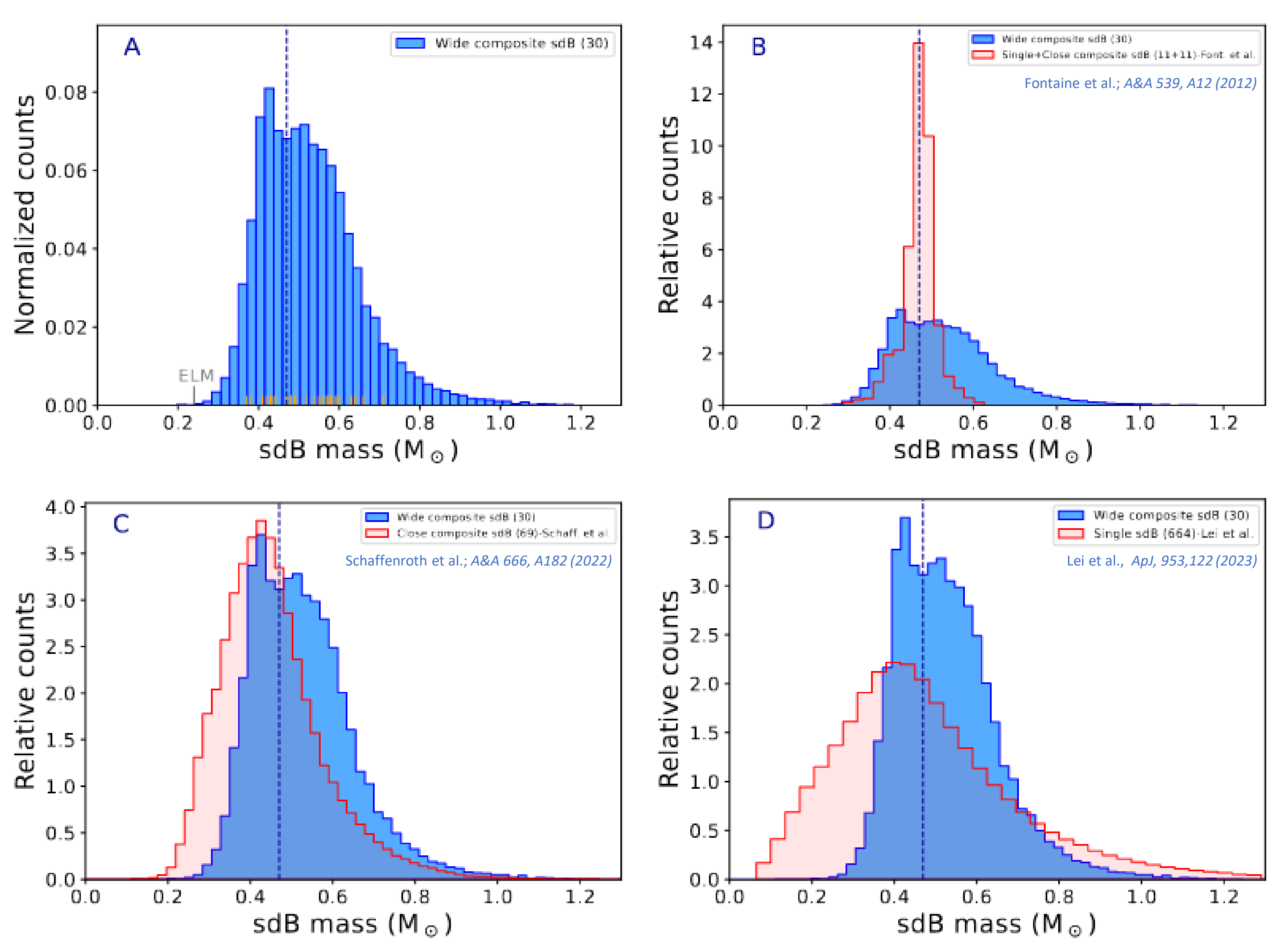

Hot subdwarfs sdB mass distributions

Molina et al. *in prep. (2024)*

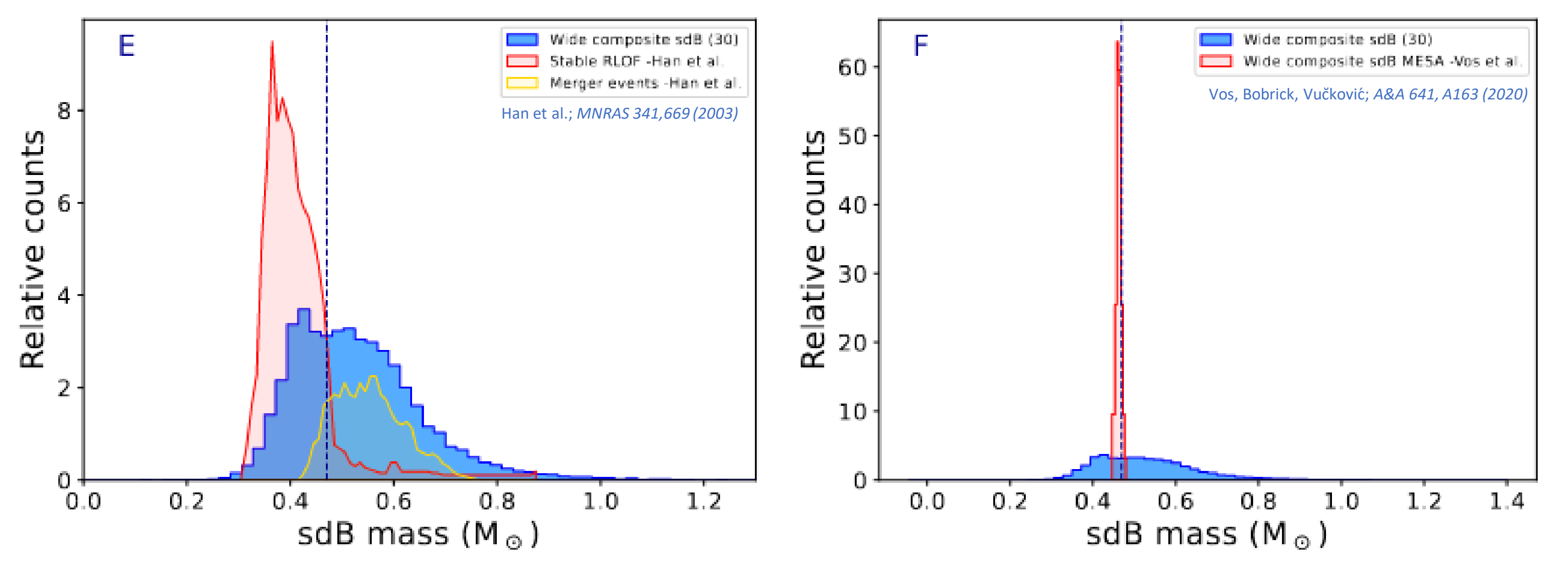

Eduardo Arencibia-Rojas et al.; *MNRAS 572, 11184 (2024)*

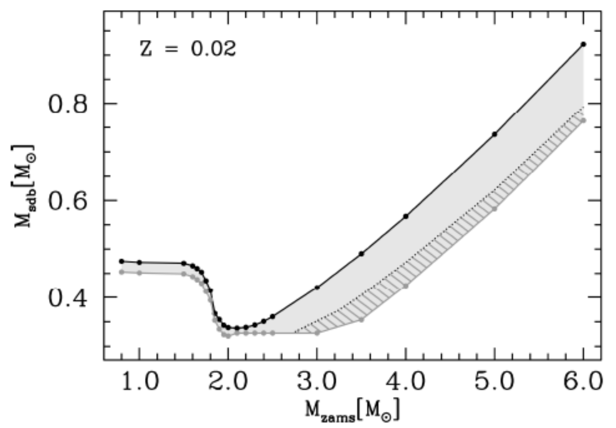

Figure 4. Maximum (black) and minimum (gray) sdB masses as a function of initial mass for the MESA models with $Z = 0.02$ and core overshooting during the MS. The gray area corresponds to the whole range of possible sdB masses, while the dashed area highlights sdBs descending from progenitors on the subgiant branch phase.

The mass range of hot subdwarf B stars from MESA simulations

Molina et al. *in prep. (2024)*

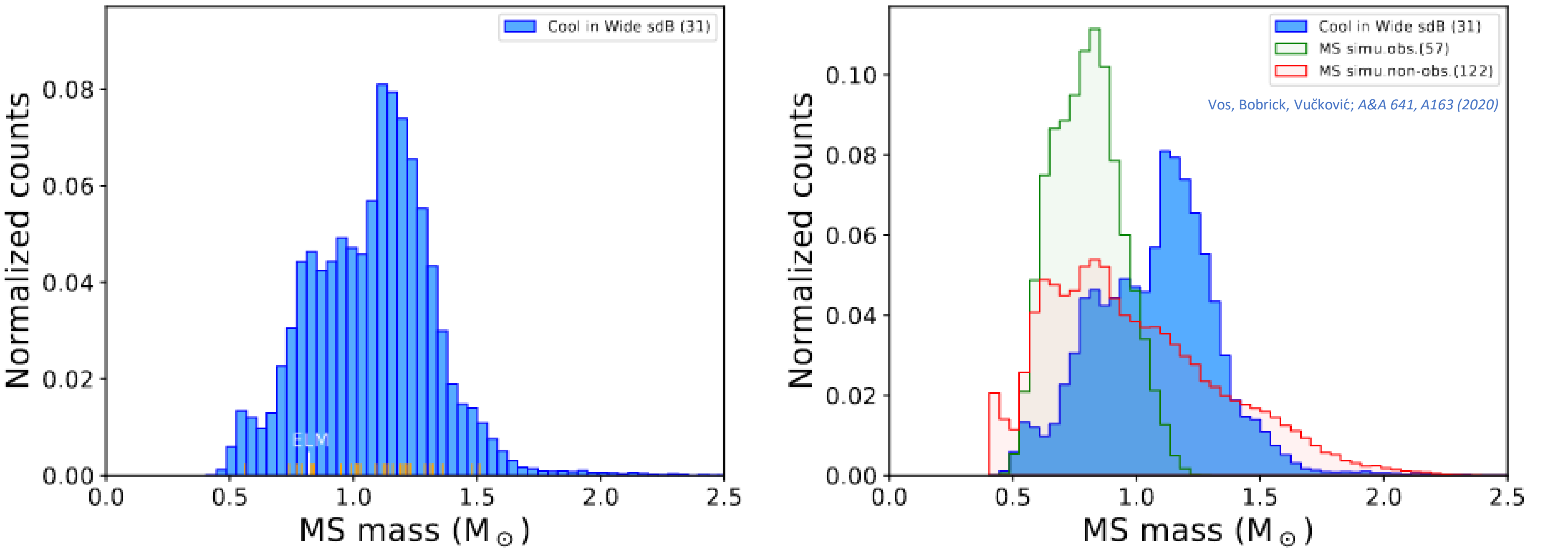

Fig. 15. *Left*: The histogram of empirical mass distribution of cool companion stars. The system BPS CS 22937-0067 is included in the sample, although in return, it does not provide a later reliable sdB mass given the poor constraint of its mass ratio parameter. The MS mass of the ELM is shown with a white tick mark, and is not included in the distribution. Probability option in y-axis. *Right*: The predicted cool companion mass distributions from the theoretical study by Vos et al. (2020) are included. They present two distributions for system simulations that meet (shaded green), or do not meet (shaded red), the double-lined observability criterion established by the authors. The bin intervals of distributions were determined from the 'Knuth' algorithm (SEABORN library).

Hot subdwarfs MS mass distribution

Lei et al., *ApJ, 942,109 (2023)*

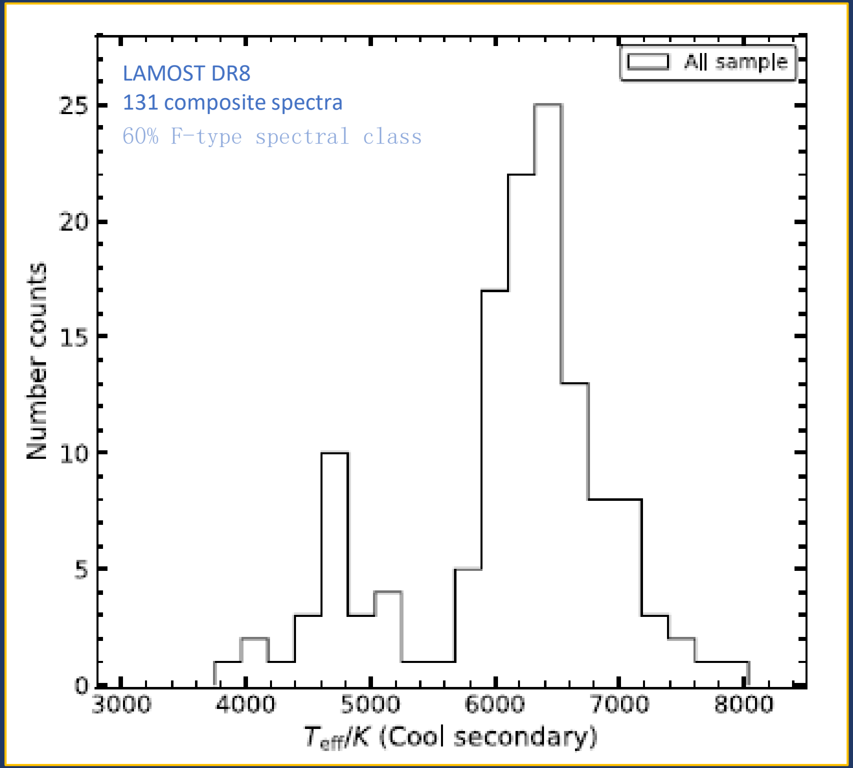

Molina et al. *in prep. (2024)*

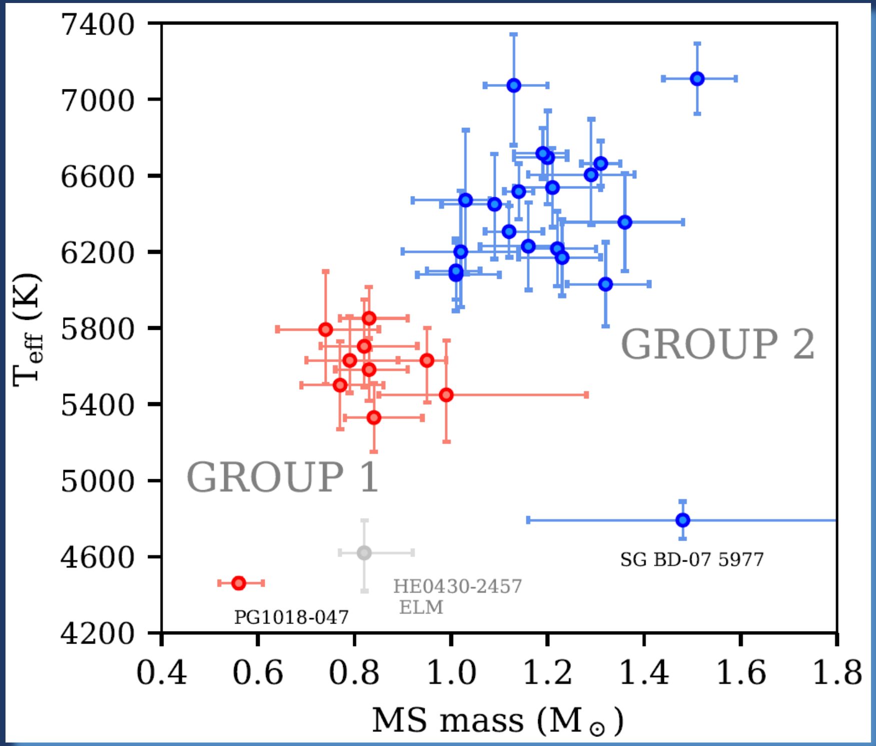

Hot subdwarfs MS mass distribution

Molina et al. *in prep. (2024)*

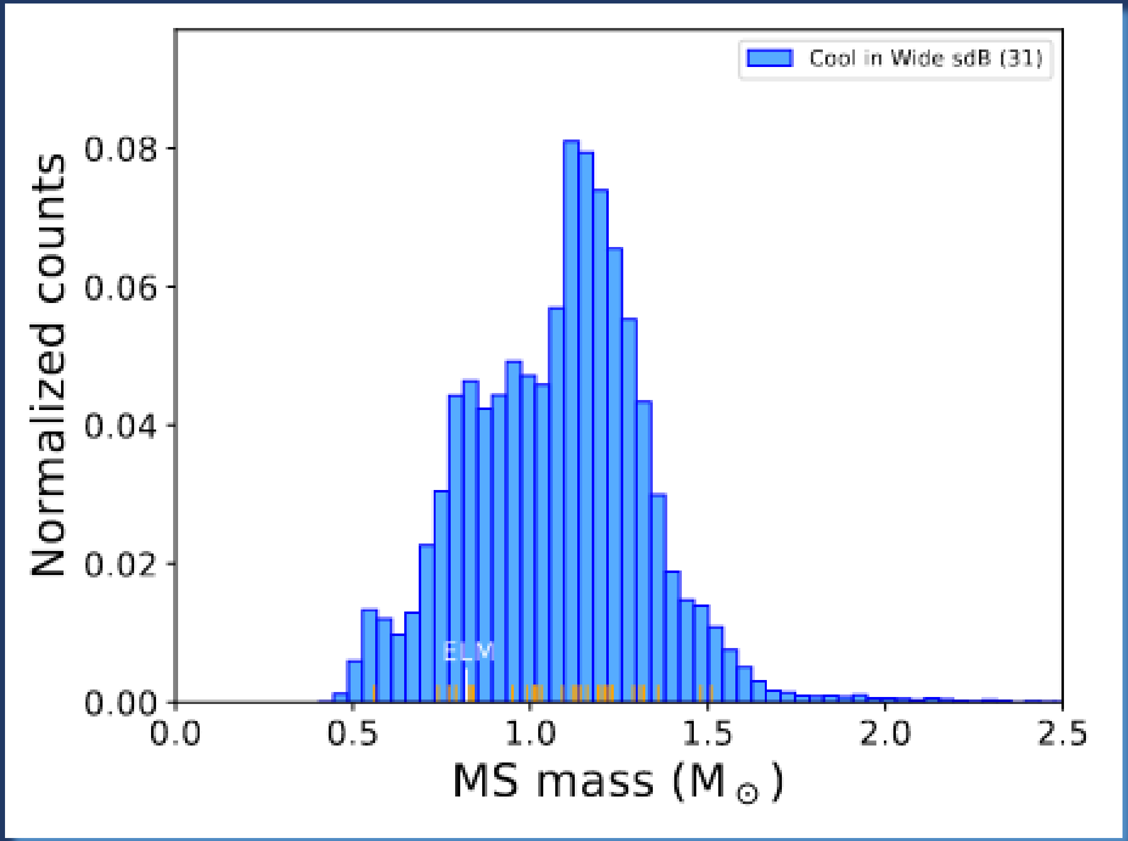

Ideal MS
"A Modern Mean Dwarf Stellar Color and Effective Temperature Sequence"
https://www.pas.rochester.edu/~emamajek/EEM_dwarf_UBVIJHK_colors_Teff.txt
Eric Mamajek --Version 2022.04.16

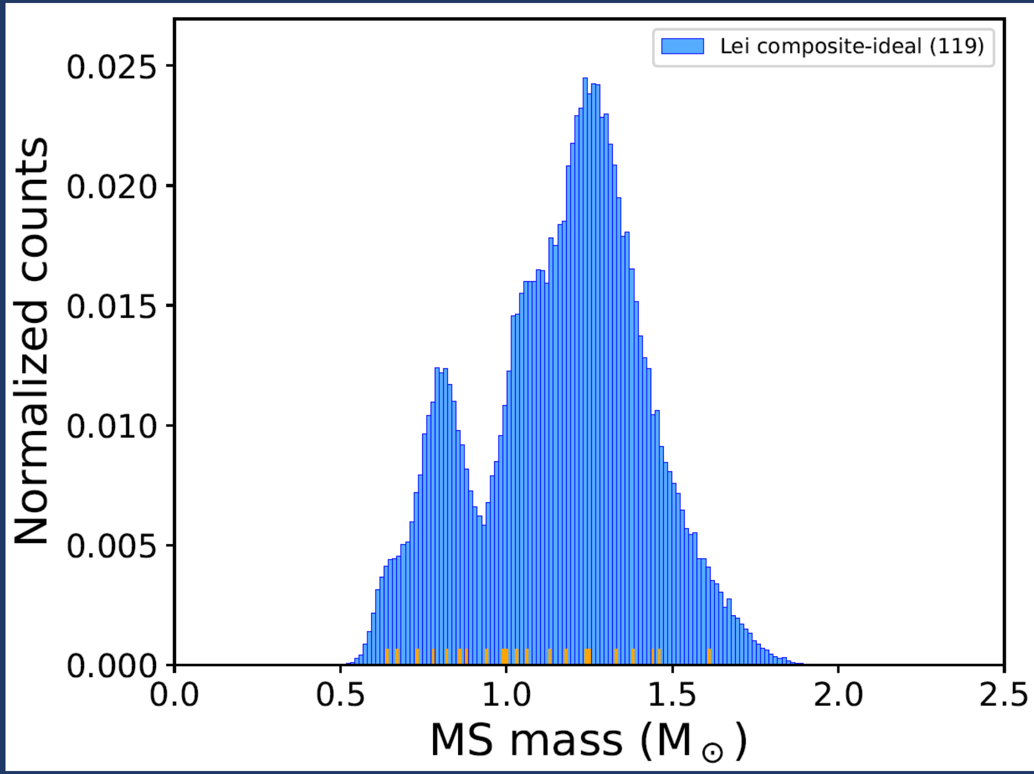

Lei et al., *ApJ, 942:109 (2023)*

Hot subdwarfs MS Rotational Periods

TESS/light curves (empirical)

https://mast.stsci.edu/portal/Mashup/Clients/Mast/Portal.htm

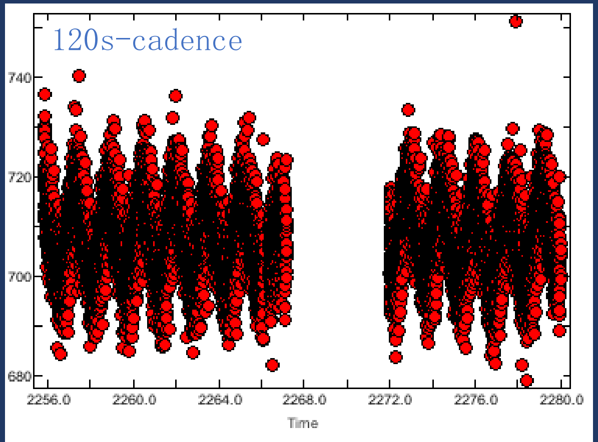

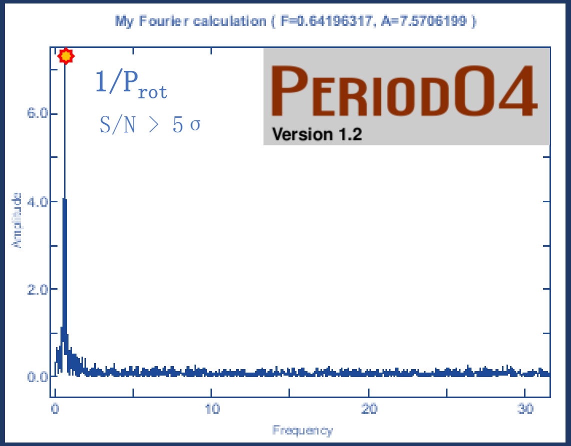

Method (calculated)

$$P_{rot} = \frac{2\pi \cdot R}{V_{rot}}$$

- Radii — Photometry study (Speedyfit)
- V.sin*i* — Atmospheric parameters study by GSSP
- Minimum MS mass — Orbital parameters radial velocity curves
- MS mass — Evolutionary study (Emcmass)
- [Fe/H] & T_{eff} — Atmospheric parameters study by GSSP

Molina et al. *in prep. (2024)*

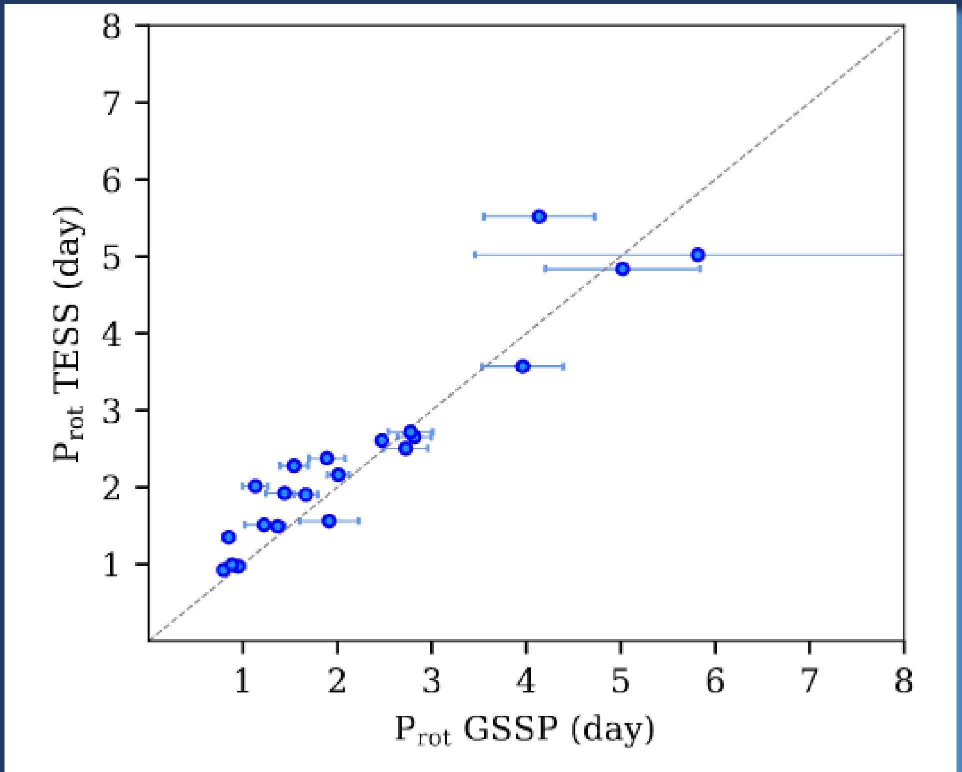

Fig. 4. Comparison of rotational periods obtained from the available light curves analysis (TESS) with significant variability (S/N > 5 σ) versus the ones obtained from the combination of different techniques in this paper (labelled here for simplicity as GSSP). Included error bars.

Hot subdwarfs MS Rotational Periods

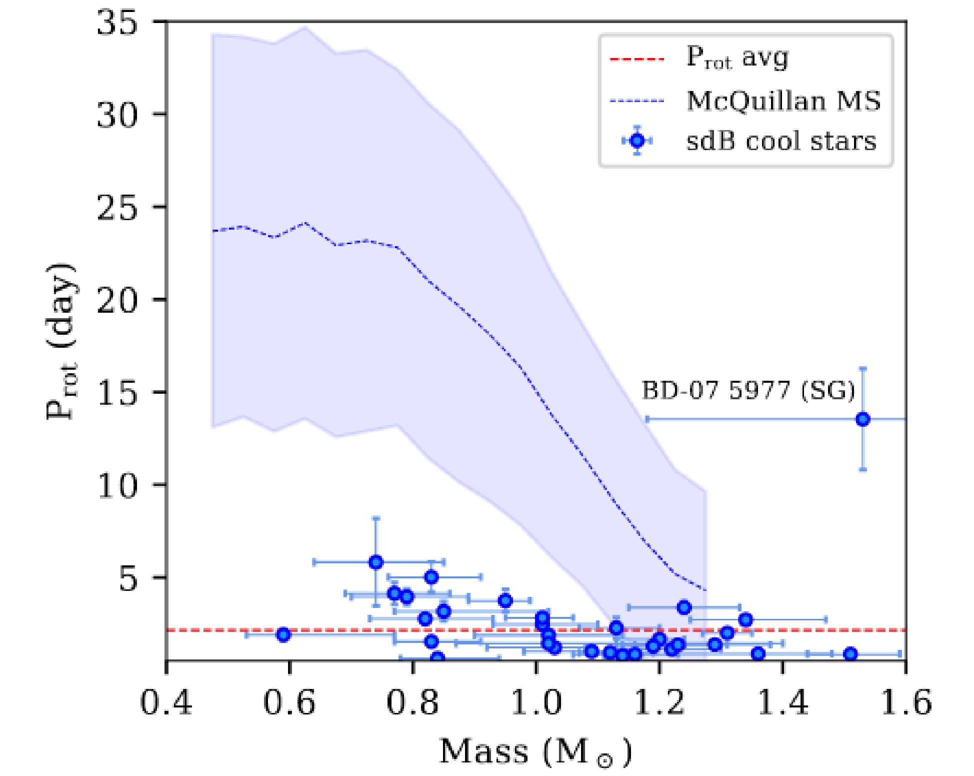

Fig. 5. The plot illustrates the average rotational periods and their standard deviation relative to stellar mass derived from the 34,030 main sequence field stars in the McQuillan et al. (2014) dataset from Kepler. This dataset specifically includes stars with T_{eff} below 6,500 K and masses less than 1.3 $M_{\odot}$. A comparative analysis is made with the MS's P_{rot} from the wide hot binary sample, included error bars. The largest P_{rot} observed in the subgiant star, suggests an increase in its moment of inertia and a slowdown of the rotation due to the expansion of the envelope (e.g. van Saders & Pinsonneault 2013). The average value of the sample, excluding the SG system, is depicted as a dashed red line.

Pelisoli's TESS avg P_{rot}

$\log P = 0.35 \pm 0.27$ (log-normal)

Pelisoli, Vos, Geier, Schaffenroth & Baran, *A&A, 642, A180 (2020)*

GSSP avg P_{rot}

$\log P = 0.34 \pm 0.31$ (log-normal)

Molina et al. *in prep. (2024)*

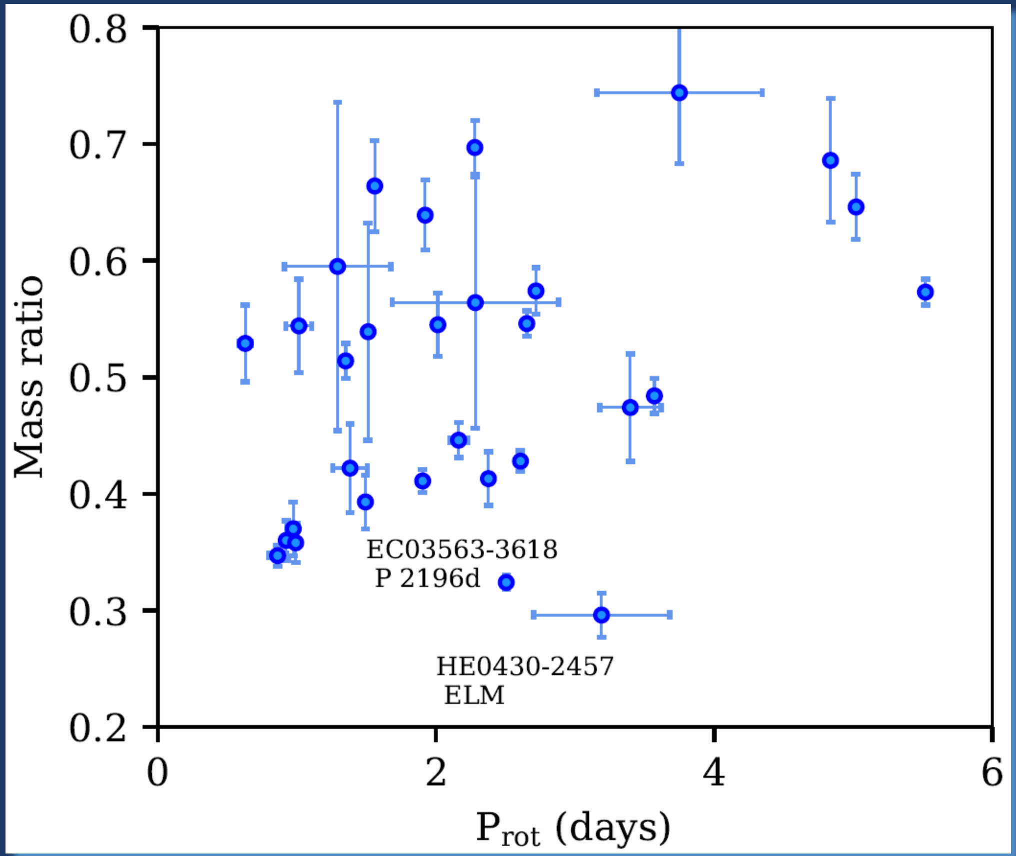

Molina et al. *in prep. (2024)*

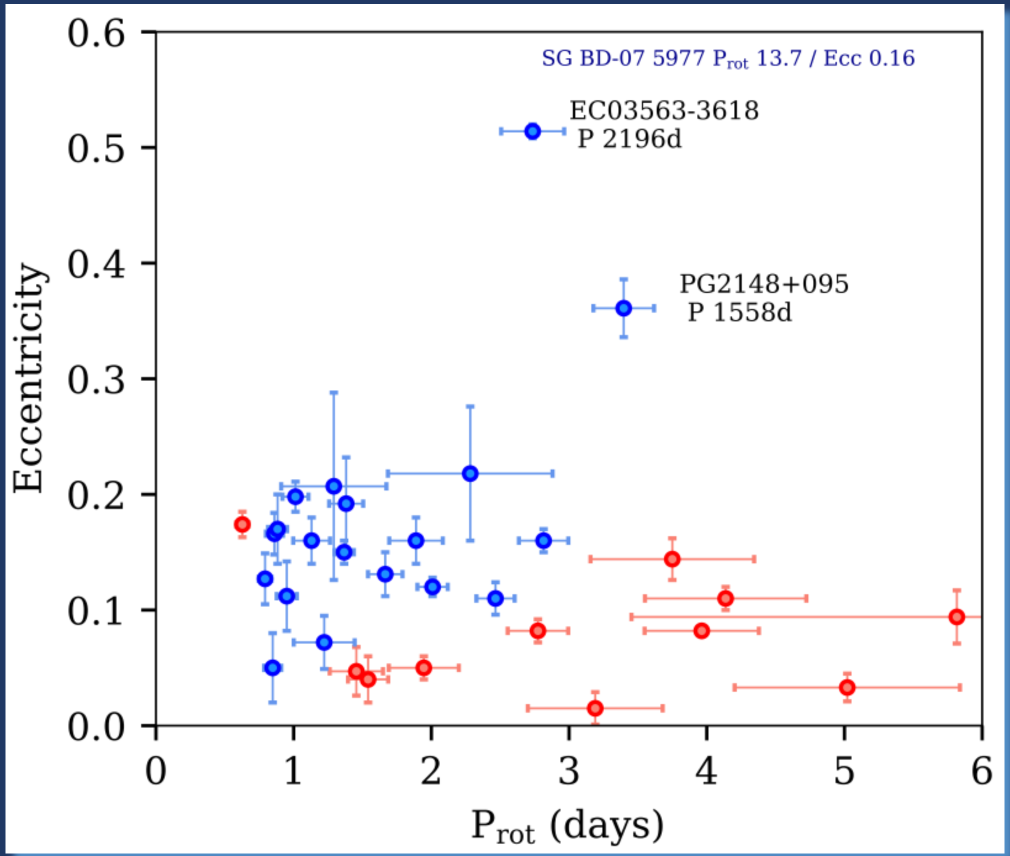

Molina et al. *in prep. (2024)*

To be continued…